31st Annual International Conference of the IEEE EMBS
Minneapolis, Minnesota, USA, September 2-6, 2009

A complete mathematical study of a 3D model of heterogeneous and anisotropic glioma evolution

Alexandros Roniotis, Kostas Marias, Vangelis Sakkalis, George D. Tsibidis, and Michalis Zervakis

Abstract— **Glioma is the most aggressive type of brain cancer. Several mathematical models have been developed towards identifying the mechanism of tumor growth. The most successful models have used variations of the diffusion-reaction equation, with the recent ones taking into account brain tissue heterogeneity and anisotropy. However, to the best of our knowledge, there hasn't been any work studying in detail the mathematical solution and implementation of the 3D diffusion model, addressing related heterogeneity and anisotropy issues. To this end, this paper introduces a complete mathematical framework on how to derive the solution of the equation using different numerical approximation of finite differences. It indicates how different proliferation rate schemes can be incorporated in this solution and presents a comparative study of different numerical approaches.**

I. Introduction

GLIOMAS are the most malignant form of brain tumor, which differ from other tumors, because of their highly aggressive and diffusive behavior. Since 90s, many important diffusive models have been introduced [1-3], with the most recent ones taking brain tissue heterogeneity and anisotropic cell migration into account. According to Jbadbi [3], the spatiotemporal diffusion equation that describes glioma growth is

$$\frac{\partial c}{\partial t} = div(\mathbf{D}(\mathbf{x})\nabla c) + f(c) \quad (1)$$

where $c(\mathbf{x},t)$ is the tumor concentration in position $\mathbf{x}$ at time t, $\mathbf{D}(\mathbf{x})$ is the diffusion tensor, i.e. a 3x3 symmetric matrix that expresses anisotropy of cell migration, ∇ and *div* are the gradient and divergence operators respectively and $f(c)$ is the net cell proliferation rate. Variant formalisms of $f(c)$ have been proposed [4], with the main ones following either the exponential law

$$f(c) = \rho c, \quad (2)$$

or the Verhulst law

$$f(c) = \rho c \frac{c_m - c}{c_m} \quad (3)$$

or Gompertz law

$$f(c) = \rho c \ln\frac{c_m}{c} \quad (4)$$

Manuscript received April 7, 2009. This work was supported in part by the EC ICT project ContraCancrum, Contract No: 223979.

A. Roniotis, V. Sakkalis, and K. Marias are with the Institute of Computer Science, Foundation for Research and Technology (FORTH), Heraklion 71110, Greece (e-mail: {roniotis; sakkalis; marias}@ics.forth.gr).

G. D. Tsibidis is with the Institute of Electronic Structure and Laser, Foundation for Research and Technology (FORTH), Heraklion 71110, Greece (e-mail: tsibidis@iesl.forth.gr).

A. Roniotis and M. Zervakis are with the Dept. of Electronic & Computer Engineering, Technical University of Crete, 73100, Chania, Greece (email: roniotis@ics.forth.gr, michalis@display.tuc.gr).

where ρ denotes the proliferation rate constant and c_m is the maximum value that c can reach.

Due to the spatial dependence of **D**, an analytical solution of (1) cannot be acquired; therefore, it has to be numerically approximated. Finite differences (FDs) are commonly used in diffusive models. By using FDs, a big system of equations arises, the iterative solution of which yields the approximated tumor cell concentration at a desired time point. Different numerical schemes for approximating partial derivatives are able to differentiate the emerging system, thus the way it is solved.

Up to now, the various implementations lack a firm mathematical background on the derivation of the system, with concrete assumptions on the approximation scheme. The main objective of this paper is to provide the direct formalism of the derived linear system, for the widely used FD schemes, namely forward Euler (FE), backward Euler (BE), Crank Nikolson (CN) and θ-methods. These formalisms are designed for 3D, heterogeneous and anisotropic brain tissue and entail the general form of $f(c)$, so that one could use any net proliferation rate. We also present how equations (2),(3) and (4) are tailored to the model. Finally, we make a comparative study of the different FD numerical schemes by analyzing experimental results.

II. METHODS

Equation (1) is a partial 2nd order differential equation. Before hunting up a direct expression of the linear system that iteratively solves it, (1) is expanded in three spatial dimensions. Assume that the diffusion tensor $\mathbf{D}(\mathbf{x})$ at a point $\mathbf{x}=(x_1, x_2, x_3)$ is:

$$\mathbf{D}(\mathbf{x}) = \begin{vmatrix} D_{11}(\mathbf{x}) & D_{12}(\mathbf{x}) & D_{13}(\mathbf{x}) \\ D_{12}(\mathbf{x}) & D_{22}(\mathbf{x}) & D_{23}(\mathbf{x}) \\ D_{13}(\mathbf{x}) & D_{23}(\mathbf{x}) & D_{33}(\mathbf{x}) \end{vmatrix} \quad (5)$$

Then, by using definitions of div and ∇, (1) becomes:

$$\frac{\partial c}{\partial t} = \sum_{i,j=1}^{3} \frac{\partial^2 c}{\partial x_i \partial x_j} D_{ij} + \sum_{i,j=1}^{3} \frac{\partial c \partial D_{ij}}{\partial x_i \partial x_j} + f(c) \quad (6)$$

The next step is to use FDs so as to approximate the solution of (6). For approximating the partial derivatives, i) FE, ii) BE, iii) θ- and iv) CN schemes are used.

A. Forward Euler Method (FE)

At first, assuming that initial and boundary conditions have been defined, we study how FE approximates the solution of (6) for a $N_X \times N_Y \times N_Z$ grid. If $c(n\Delta T, i\Delta X, j\Delta Y, k\Delta Z) \equiv C_{i,j,k}^{n}$, $D_{pq}(i\Delta X, j\Delta Y, k\Delta Z) \equiv D_{pq,i,j,k}$, $i \in \{0, \dots, N_X - 1\}$, $j \in \{0, \dots, N_Y - 1\}$, $k \in \{0, \dots, N_Z - 1\}$ and $p, q \in \{1,2,3\}$, then the partial derivatives of (6) in point

(iΔX,jΔY,kΔZ) can be approximated as

$$\frac{\partial c}{\partial t} \to \frac{C_{i,j,k}^{n+1}-C_{i,j,k}^{n}}{\Delta T}$$
$$\frac{\partial c}{\partial x} \to \frac{C_{i+1,j,k}^{n}-C_{i-1,j,k}^{n}}{2\Delta X}$$
$$\frac{\partial^2 c}{\partial x^2} \to \frac{C_{i+1,j,k}^{n}-2C_{i,j,k}^{n}+C_{i-1,j,k}^{n}}{\Delta X^2}$$
$$\frac{\partial^2 c}{\partial x \partial y} \to \frac{C_{i+1,j+1,k}^{n}+C_{i-1,j-1,k}^{n}-C_{i+1,j-1,k}^{n}-C_{i-1,j+1,k}^{n}}{4\Delta X\Delta Y}$$
$$\frac{D_{pq}}{\partial x} \to \frac{D_{pq,i+1,j,k}-D_{pq,i-1,j,k}}{2\Delta X} \quad (7)$$

and similarly for $\frac{\partial c}{\partial y}, \frac{\partial c}{\partial z}, \frac{\partial^2 c}{\partial y^2}, \frac{\partial^2 c}{\partial z^2}, \frac{\partial^2 c}{\partial x \partial z}, \frac{\partial^2 c}{\partial y \partial z}, \frac{D_{pq}}{\partial y}$ and $\frac{D_{pq}}{\partial z}$. If any of the neighboring $C_{i,j,k}^{n}$ is a boundary point, then its value will be as initially defined. Continuing, by substituting the approximations (7) to (6), we derive:

$$\begin{aligned}\frac{C_{i,j,k}^{n+1}-C_{i,j,k}^{n}}{\Delta T} &= f\left(C_{i,j,k}^{n}\right) + A(i,j,k)_0 C_{i-1,j-1,k}^{n} + A(i,j,k)_1 C_{i-1,j,k-1}^{n} \\ &+ A(i,j,k)_2 C_{i-1,j,k}^{n} + A(i,j,k)_3 C_{i-1,j,k+1}^{n} + A(i,j,k)_4 C_{i-1,j+1,k}^{n} \\ &+ A(i,j,k)_5 C_{i,j-1,k-1}^{n} + A(i,j,k)_6 C_{i,j-1,k}^{n} + A(i,j,k)_7 C_{i,j-1,k+1}^{n} \\ &+ A(i,j,k)_3 C_{i-1,j,k+1}^{n} + A(i,j,k)_9 C_{i,j,k}^{n} + A(i,j,k)_{10} C_{i,j,k+1}^{n} \\ &+ A(i,j,k)_{11} C_{i,j+1,k-1}^{n} + A(i,j,k)_{12} C_{i,j+1,k}^{n} + A(i,j,k)_{13} C_{i,j+1,k+1}^{n} \\ &+ A(i,j,k)_{14} C_{i+1,j-1,k}^{n} + A(i,j,k)_{15} C_{i+1,j,k-1}^{n} + A(i,j,k)_{16} C_{i+1,j,k}^{n} \\ &+ A(i,j,k)_{17} C_{i+1,j,k+1}^{n} + A(i,j,k)_{18} C_{i+1,j+1,k}^{n} \quad (8)\end{aligned}$$

or equivalently:

$$\frac{C_{i,j,k}^{n+1}-C_{i,j,k}^{n}}{\Delta T} = [A(i,j,k)_0 \quad \dots \quad A(i,j,k)_{18}] \begin{bmatrix} C_{i-1,j-1,k}^{n} \\ \dots \\ C_{i+1,j+1,k}^{n} \end{bmatrix} + f\left(C_{i,j,k}^{n}\right) \quad (9)$$

where

$$\begin{aligned}A(i,j,k)_2 &= \frac{D_{11,i,j,k}}{\Delta X^2} - \frac{D_{11,i+1,j,k}-D_{11,i-1,j,k}}{4\Delta X^2} \\ &- \frac{D_{21,i,j+1,k}-D_{21,i,j-1,k}}{4\Delta X\Delta Y} - \frac{D_{31,i,j,k+1}-D_{31,i,j,k-1}}{4\Delta X\Delta Z} \\ A(i,j,k)_6 &= \frac{D_{22,i,j,k}}{\Delta Y^2} - \frac{D_{12,i+1,j,k}-D_{12,i-1,j,k}}{4\Delta X\Delta Y} \\ &- \frac{D_{22,i,j+1,k}-D_{22,i,j-1,k}}{4\Delta Y^2} - \frac{D_{32,i,j,k+1}-D_{32,i,j,k-1}}{4\Delta Y\Delta Z} \\ A(i,j,k)_8 &= \frac{D_{33,i,j,k}}{\Delta Z^2} - \frac{D_{13,i+1,j,k}-D_{13,i-1,j,k}}{4\Delta X\Delta Z} \\ &- \frac{D_{23,i,j+1,k}-D_{23,i,j-1,k}}{4\Delta Y\Delta Z} - \frac{D_{33,i,j,k+1}-D_{33,i,j,k-1}}{4\Delta Z^2} \\ A(i,j,k)_{10} &= \frac{D_{33,i,j,k}}{\Delta Z^2} + \frac{D_{13,i+1,j,k}-D_{13,i-1,j,k}}{4\Delta X\Delta Z} \\ &+ \frac{D_{23,i,j+1,k}-D_{23,i,j-1,k}}{4\Delta Y\Delta Z} + \frac{D_{33,i,j,k+1}-D_{33,i,j,k-1}}{4\Delta Z^2} \\ A(i,j,k)_{12} &= \frac{D_{22,i,j,k}}{\Delta Y^2} + \frac{D_{12,i+1,j,k}-D_{12,i-1,j,k}}{4\Delta X\Delta Y} \\ &+ \frac{D_{22,i,j+1,k}-D_{22,i,j-1,k}}{4\Delta Y^2} + \frac{D_{32,i,j,k+1}-D_{32,i,j,k-1}}{4\Delta Y\Delta Z} \\ A(i,j,k)_{16} &= \frac{D_{11,i,j,k}}{\Delta X^2} + \frac{D_{11,i+1,j,k}-D_{11,i-1,j,k}}{4\Delta X^2} \\ &+ \frac{D_{21,i,j+1,k}-D_{21,i,j-1,k}}{4\Delta X\Delta Y} + \frac{D_{31,i,j,k+1}-D_{31,i,j,k-1}}{4\Delta X\Delta Z} \\ A(i,j,k)_0 &= -A(i,j,k)_4 = -A(i,j,k)_{14} = A(i,j,k)_{18} = \frac{D_{12,i,j,k}}{2\Delta X\Delta Y} \\ A(i,j,k)_1 &= -A(i,j,k)_3 = -A(i,j,k)_{15} = A(i,j,k)_{17} = \frac{D_{13,i,j,k}}{2\Delta X\Delta Z} \\ A(i,j,k)_5 &= -A(i,j,k)_7 = -A(i,j,k)_{11} = A(i,j,k)_{13} = \frac{D_{23,i,j,k}}{2\Delta Y\Delta Z} \\ A(i,j,k)_9 &= -2\frac{D_{11,i,j,k}}{\Delta X^2} - 2\frac{D_{22,i,j,k}}{\Delta Y^2} - 2\frac{D_{33,i,j,k}}{\Delta Z^2} \quad (10)\end{aligned}$$

If the vectorized version of $C_{i,j,k}^{n}$ at time mΔT is taken, as

$$\mathbf{C}^{\mathrm{m}} \equiv \left[\underbrace{C_{0,0,0}^{m} \quad C_{0,0,1}^{m} \quad \dots \quad C_{0,1,0}^{m} \quad \dots \quad C_{N_X-1,N_Y-1,N_Z-1}^{m}}_{N_X N_Y N_Z} \right]^T \quad (11)$$

then, the overall solution of the equation at time $n+1$, for given $\mathbf{C}^0$, can be found by solving iteratively $\frac{\mathbf{C}^{n+1}-\mathbf{C}^{\mathrm{n}}}{\Delta T} = \mathbf{A}\mathbf{C}^{\mathrm{n}} + F(\mathbf{C}^{\mathrm{n}})$ where $\mathbf{A}$ is a $N_X N_Y N_Z \times N_X N_Y N_Z$ matrix with its elements defined as:

$$\mathrm{A}_{ml} = \begin{cases} A(i,j,k)_0, l = m - N_Y N_Z - N_Z & A(i,j,k)_{10}, l = m+1 \\ A(i,j,k)_1, l = m - N_Y N_Z - 1 & A(i,j,k)_{11}, l = m + N_Z - 1 \\ A(i,j,k)_2, l = m - N_Y N_Z & A(i,j,k)_{12}, l = m + N_Z \\ A(i,j,k)_3, l = m - N_Y N_Z + 1 & A(i,j,k)_{13}, l = m + N_Z + 1 \\ A(i,j,k)_4, l = m - N_Y N_Z + N_Z & A(i,j,k)_{14}, l = m + N_Y N_Z - N_Z \\ A(i,j,k)_5, l = m - N_Z - 1 & A(i,j,k)_{15}, l = m + N_Y N_Z - 1 \\ A(i,j,k)_6, l = m - N_Z & A(i,j,k)_{16}, l = m + N_Y N_Z \\ A(i,j,k)_7, l = m - N_Z + 1 & A(i,j,k)_{17}, l = m + N_Y N_Z + 1 \\ A(i,j,k)_8, l = m - 1 & A(i,j,k)_{18}, l = m + N_Y N_Z + N_Z \\ A(i,j,k)_9, l = m & 0, otherwise \end{cases}$$

where:

$$m = iN_Y N_Z + jN_Z + k \text{ and } m, l \in \{0, \dots, N_X N_Y N_Z - 1\} \quad (12)$$

and F a *vectorization operator* that vectorizes $f(C_{i,j,k}^{n})$ as

$$F(\boldsymbol{C}^{n}) \equiv \left[f\left(C_{0,0,0}^{n}\right) \quad f\left(C_{0,0,1}^{n}\right) \quad \dots \quad f\left(C_{N_X-1,N_Y-1,N_Z-1}^{n}\right) \right]^T \quad (13)$$

$\mathbf{A}$ is a $N_X N_Y N_Z \times N_X N_Y N_Z$ symmetric, sparse, 19-diagonal matrix, with its form being visualized in Fig.1, where all light gray areas have zero values.

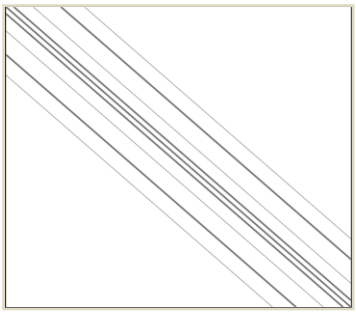

Fig. 1. Sparse Matrix **A**: White areas have zero values, thick lines are 3 diagonals in a row and thin lines are single diagonals.

After having acquired $\mathbf{A}$, a direct solution can be found by iteratively calculating

$$\mathbf{C}^{n+1} = (\mathbf{I} + \Delta T\mathbf{A})\mathbf{C}^{\mathrm{n}} + \Delta T \cdot F(\mathbf{C}^{\mathrm{n}}) \quad (14)$$

where $\mathbf{I}$ is the $N_X N_Y N_Z \times N_X N_Y N_Z$ identity matrix. This is the solution of the FE. This is called *forward*, because the next-time approximation of concentration can be directly estimated as a linear combination of the previous-time approximation and is easy to implement, but numerical stability has to be ensured. As proven in [5], this method is stable giving reliable results when

$$\Delta T \leq min_{x,y,z}\left(\frac{1}{2\left(\frac{D_{11}(x,y,z)}{\Delta X^2} + \frac{D_{22}(x,y,z)}{\Delta Y^2} + \frac{D_{33}(x,y,z)}{\Delta Z^2}\right)} \right) \quad (15)$$

B. Backward Euler (BE)

Similarly, the density of glioma cells at time t, using BE, can be derived by iteratively solving the system:

$$\left(\mathbf{I} - \Delta T\mathbf{A}\right)\mathbf{C}^{n+1} - \Delta T \cdot F\left(\mathbf{C}^{\mathrm{n+1}}\right) = \mathbf{C}^{\mathrm{n}} \quad (16)$$

till time t is reached, with $\mathbf{A}$ and F being the same with (12) and (13) respectively. In each iteration the system can be expressed with a big, sparse, symmetric and positive definite matrix; an iterative method for solving

linear systems, e.g. the conjugate gradient method can be used. Unconditional stability and accuracy are advantages of this method, whereas computational and storage load that has to be considered [6].

C. θ-methods/Crank Nikolson (CN)

The θ-methods use a balancing parameter θ∈ [0,1], so as to combine forward and backward numerical schemes concurrently. By using θ-methods we get

$$(\mathbf{I}\text{-}\theta\Delta T\mathbf{A})\mathbf{C}^{n+1} - \theta\Delta T \cdot F(\mathbf{C}^{n+1}) = (\mathbf{I}\text{+}q\Delta T\mathbf{A})\mathbf{C}^{n} + q\Delta T \cdot F(\mathbf{C}^{n}) \quad (17)$$

where $q = 1 - \theta$. As in BE, a method for solving linear systems is required. The θ-methods are flexible due to choice of parameter θ but higher computational and storage load are required [6]. CN is a θ-method for θ=½.

In Table I, the formulation of the iterative linear systems that produce the approximated solution of (6) is presented according to various selected methods. Based on this, we have implemented models for glioma growth, directly in 3D using C++ (the authors can be contacted for more details).

TABLE I
DIRECT EXPRESSIONS OF THE ITERATIVE LINEAR SYSTEMS

Numerical scheme	Iterative linear system solving (6)
Forward Euler	$\mathbf{C}^{n+1} = (\mathbf{I}\text{+}\Delta T\mathbf{A})\mathbf{C}^{n} + \Delta T \cdot F(\mathbf{C}^{n})$
Backward Euler	$(\mathbf{I}\text{-}\Delta T\mathbf{A})\mathbf{C}^{n+1} - \Delta T \cdot F(\mathbf{C}^{n+1}) = \mathbf{C}^{n}$
θ-methods	$(\mathbf{I}\text{-}\theta\Delta T\mathbf{A})\mathbf{C}^{n+1} - \theta\Delta T \cdot F(\mathbf{C}^{n+1}) = (\mathbf{I}\text{+}(1-\theta)\Delta T\mathbf{A})\mathbf{C}^{n} + (1-\theta)\Delta T \cdot F(\mathbf{C}^{n})$

D. Vectorization Operator

It is interesting to study how operator F is chosen for the mainly used proliferation rates of (2),(3) and (4). If the net proliferation rate is given by (2) holds, then according to (13):

$$F(\boldsymbol{C}^n) = \left[\rho C^n_{0,0,0} \quad \rho C^n_{0,0,1} \quad \dots \quad \rho C^n_{N_X-1,N_Y-1,N_Z-1}\right]^T \quad (18)$$

or equivalently:

$$F(\boldsymbol{C}^n) = \rho \boldsymbol{C}^n \quad (19)$$

Next, if the net proliferation rate is given by (3), then:

$$F(\boldsymbol{C}^n) = \left[\rho C^n_{0,0,0}\frac{c_m - C^n_{0,0,0}}{c_m} \quad \rho C^n_{0,0,1}\frac{c_m - C^n_{0,0,1}}{c_m} \quad \dots\right]^T \quad (20)$$

or equivalently:

$$F(\boldsymbol{C}^n) = \frac{\rho}{c_m} diag(\boldsymbol{C}^n)(c_m \mathbf{1}^{1\times N_X N_Y N_Z} - \boldsymbol{C}^n). \quad (21)$$

The definitions of $diag$ and $\mathbf{1}^{1\times N}$ are given in Table 2. Lastly, if the net proliferation rate is given by (4) holds, then according to (13):

$$F(\boldsymbol{C}^n) = \left[\rho C^n_{0,0,0}\ln\frac{c_m}{C^n_{0,0,0}} \quad \rho C^n_{0,0,1}\ln\frac{c_m}{C^n_{0,0,1}} \quad \dots\right]^T \quad (22)$$

or equivalently:

$$F(\boldsymbol{C}^n) = \rho diag\left(ln(c_m \mathbf{1}^{1\times N_X N_Y N_Z}) - ln(\boldsymbol{C}^n)\right)\boldsymbol{C}^n \quad (23)$$

In Table II, a summary of vectorization operator for the commonly used proliferation rates is presented.

III. RESULTS AND DISCUSSION

In order to study the performance of the different numerical schemes presented, a simplified test case of the pure diffusion equation is used, for which there is a known analytical continuous expression of the solution.

TABLE II
VECTORIZATION OPERATOR FOR DIFFERENT PROLIFERATION RATES

Proliferation Rate	Constant Rate *f(c)*	Vectorization Operator $F(\mathbf{C}^n)$
Exponential	ρc	$\rho \boldsymbol{C}^n$
Verhulst (logistic)	$\rho c\frac{c_m - c}{c_m}$	$\frac{\rho}{c_m} diag(\boldsymbol{C}^n)(c_m \mathbf{1}^{1\times N_X N_Y N_Z} - \boldsymbol{C}^n)$
Gompertz	$\rho c\ln\frac{c}{c_m}$	$\rho diag\left(ln(c_m \mathbf{1}^{1\times N_X N_Y N_Z}) - ln(\boldsymbol{C}^n)\right)\boldsymbol{C}^n$

$$diag\begin{bmatrix} x_1 \\ x_2 \\ \dots \\ x_N \end{bmatrix} = \begin{bmatrix} x_1 & 0 & \dots & 0 \\ 0 & x_2 & \dots & 0 \\ \dots & \dots & \dots & \dots \\ 0 & 0 & \dots & x_N \end{bmatrix} \qquad \mathbf{1}^{1\times N} = \left.\begin{bmatrix} 1 \\ 1 \\ \dots \\ 1 \\ 1 \end{bmatrix}\right\} N$$

Hence, the magnitude of each numerical scheme deviation from the real solution can be studied, which serves here as 'ground truth' for validating our numerical approximations.

A. Spherical homogeneous test tumor

To validate our methodology, it is assumed that tumor growth in 3D, unbounded, isotropic (i.e. D is constant) and homogeneous region exhibits a pure diffusion behavior (i.e. $f(c) = 0$). The tumor has initially a concentration c_0 and it is constrained in a sphere of radius a (Fig. 2). Due to symmetry, the concentration of glioma depends only on the distance from the center of the sphere r and it is given by the expression [7]:

$$C(r,t) = \frac{1}{2}c_0\left(erf\left(\frac{a-r}{2\sqrt{Dt}}\right) + erf\left(\frac{a+r}{2\sqrt{Dt}}\right)\right) - \frac{c_0}{r}\sqrt{\frac{Dt}{\pi}}\left(exp\left(-\frac{(a-r)^2}{4Dt}\right) - exp\left(-\frac{(a+r)^2}{4Dt}\right)\right) \quad (24)$$

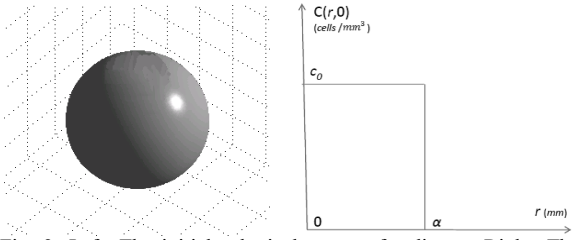

Fig. 2. Left: The initial spherical tumor of radius $\boldsymbol{a}$. Right: The initial tumor concentration according to r at time t=0

B. Testing and Simulation Description

In our tests, the model is adapted to approximate (24), by using the following parameters: $f(c) = 0$, $D = 0.5\ mm^2/day$, $a = 10\ mm$, $\Delta X = \Delta Y = \Delta Z = 1\ mm$, $\Delta T = 0.25\ days$, $N_X = N_Y = N_Z = 128$ points and $c_0 = 10^4\ cells/mm^3$. Five different simulations were run for 200 days, using FE, three θ-methods for θ=0.25, θ=0.5 (CN) , θ=0.75, and BE performed on a Pentium 4 at 3.8 GHz.

In Fig.3, the evolution of cell concentration in time is presented, with respect to r, with lines corresponding to results from analytical expression (24), while dots representing what simulation with CN yields. Fig. 3 shows a very good agreement between these results; however a more rigorous investigation would require an error estimation analysis.

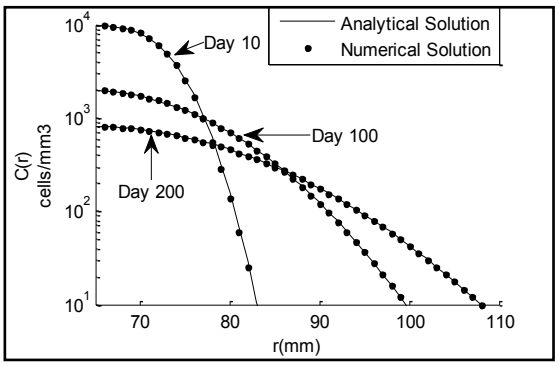

Fig. 3. The evolution of $C(r)$ after 10, 100 and 200 days

C. Error Estimation

In order to estimate the error that each scheme yields the normalized mean absolute error e is introduced. Due to symmetry, e at time $t = n\Delta T$ is computed as

$$e = \frac{1}{128}\sum_{i=1}^{128}\left|\frac{C(i\Delta X, n\Delta T) - C^{n}_{i,64,64}}{c_0}\right| \times 100\% \qquad (25)$$

TABLE III
ERROR e AFTER 10, 100 AND 200 DAYS

Scheme	10 days	100 days	200 days	Simulation Time
FE	**6.36%**	**0.89%**	**0.57%**	3'53"
θ-method (θ=0.25)	**9.73%**	**0.43%**	**0.33%**	18'13"
CN	**9.83%**	**0.91%**	**0.23%**	19'01"
θ-method (θ=0.75)	**10.17%**	**1.43%**	**0.35%**	20'16"
BE	**11.33%**	**1.95%**	**0.50%**	22'31"

In Table III, the estimated e for each scheme on day 10, 100 and 200 of simulation is reported. Moreover, the overall simulation times are also reported. The highest e for all five schemes is on 10th day, while it decreases to values $< 0.6\%$ on the 200th day. FE error is the lowest on 10th day, i.e. 6.36%, but overcomes all other schemes on 200th day, reaching 0.57% at the 200th day. CN is the scheme that reaches the lowest error value at 200th day at 0.23%. In Fig.4, a logarithmic graph of e in time is presented, for each scheme. It is noticeable that all schemes initially produce higher errors. A possible explanation is that the initial concentration $C(r,0)$ has an abrupt step descent at r=10mm, as seen in Fig. 2 (right). This makes the approximation of the partial derivatives at the edge of this step erroneous for all schemes. However, as simulation continues, all schemes tend to significantly decrease e. Continuing, one can observe that e decreases to values <1% on day 40, 75, 94, 143 and 156 for FE, 0.25-method, CN, 0.75-method and BE respectively. FE error has a remarkable descent till day 42, but later decreases smoothly and finally overcomes all other schemes. BE produces the highest error, till day 186, when FE overcomes it. As expected, approximation with θ-methods is more accurate than BE throughout all days and more accurate than FE in most time. θ-method for θ=0.25 initially tends to have a steep descent to error 0.3%, but later reaches a balancing value higher than CN. θ-method for θ=0.75 has a smoother

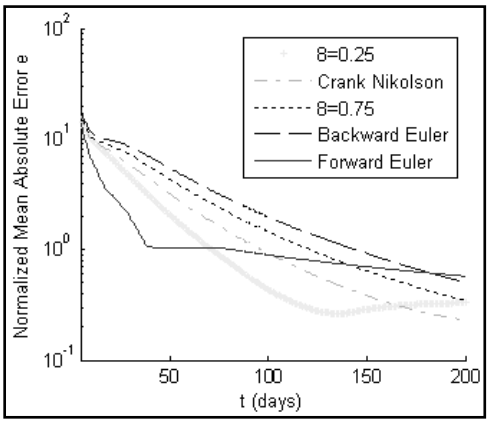

Fig. 4. Logarithmic visualization of error e in time

descent, being always higher than CN. Lastly, CN (θ=0.5) seems to have the best general performance, reaching the lowest error 0.23% on day 200.

Thus, CN seems to yield more accurate approximations of $C(r,t)$. However, if there is room for sacrificing accuracy for faster model simulations, then FE should be used, since from Table III it's derived that FE is 4.63 times faster than CN. Even if one chooses FE, that is the worst case scenario, error e doesn't overcome 0.6%

IV. CONCLUSION

This paper presents a complete, FDs' based, framework for the mathematical solving of the anisotropic, heterogeneous and 3D diffusion-reaction equation simulating either the growth of glioma or other phenomena where diffusive models are applicable. Moreover, the introduction of the vectorization operator gives the flexibility to include any proliferation rate into the model. Lastly, a performance study of different numerical schemes is presented based on an analytical expression that can be derived for the pure diffusion equation.

REFERENCES

[1] P. Tracqui, "From passive diffusion to active cellular migration in mathematical models of tumor invasion," *Acta Bibliotheoretica*, vol. 43, pp 443-464, 1995.

[2] K. R. Swanson, E. C. Alvord, and J. D. Murray, "A Quantitative Model for Differential Motility of Gliomas in Grey and White Matter," *Cell Proliferation,* vol. 33, no. 5, pp. 317-330, 2000.

[3] S. Jbabdi, E. Mandonnet, and H. Duffau, "Simulation of anisotropic growth of low-grade gliomas using diffusion tensor imaging," *Magn Reson Med*, vol. 54, pp. 616-24, 2005.

[4] M. Marusic, Z. Bajzer, J. P. Freyer, and S. Vuk-Palovic, "Analysis of growth of multicellular tumour spheroids by mathematical models," *Cell Prolif*, vol. 27, pp. 73-94, 1994.

[5] S. Puwal, and B. J. Roth, "Forward Euler Stability of the Bidomain Model of Cardiac Tissue," *IEEE Transactions on Biom. Eng.,* vol. 54, no. 5, pp. 951-953, 2005.

[6] S. Teukolsky, W. Vetterling, B. Flannery, Numerical Recipes: The Art of Scientific Computing (Third Edition), Cambridge University Press, NY, 2007.

[7] J. Crank, The Mathematics of Diffusion (Second Edition), Oxford University Press, NY, 1975.